Bioconjugate Chemistry

Article

pubs.acs.org/bc

Exploring Passive Clearing for 3D Optical Imaging of Nanoparticles in Intact Tissues

Shrey Sindhwani,[†,#] Abdullah Muhammad Syed,[†,#] Stefan Wilhelm,[†] and Warren C. W. Chan[*,†,‡,§,∥,⊥]

[†]Institute of Biomaterials and Biomedical Engineering, Rosebrugh Building, Room 407, 164 College Street, Toronto, Ontario M5S 3G9, Canada

[‡]Department of Chemistry, University of Toronto, 80 Saint George Street, Toronto, Ontario M5S 3H6, Canada

[§]Terrence Donnelly Centre for Cellular and Biomolecular Research, University of Toronto, 160 College Street, Room 230, Toronto, Ontario M5S 3E1, Canada

[∥]Department of Chemical Engineering, University of Toronto, 200 College Street, Toronto, Ontario M5S 3E5, Canada

[⊥]Department of Material Science and Engineering, University of Toronto, 160 College Street, Room 450, Toronto, Ontario M5S 3E1, Canada

Supporting Information

ABSTRACT: The three-dimensional (3D) optical imaging of nanoparticle distribution within cells and tissues can provide insights into barriers to nanoparticle transport in vivo. However, this approach requires the preparation of optically transparent samples using harsh chemical and physical methods, which can lead to a significant loss of nanoparticles and decreased sensitivity of subsequent analyses. Here, we investigate the influence of electrophoresis and clearing time on nanoparticle retention within intact tissues and the impact of these factors on the final 3D image quality. Our findings reveal that longer clearing times lead to a loss of nanoparticles but improved transparency of tissues. We discovered that passive clearing improved nanoparticle retention 2-fold compared to results from electrophoretic clearing. Using the passive clearing approach, we were able to observe a small population of nanoparticles undergoing hepatobiliary clearance, which could not be observed in liver tissues that were prepared by electrophoretic clearing. This strategy enables researchers to visualize the interface between nanomaterials and their surrounding biological environment with high sensitivity, which enables quantitative and unbiased analysis for guiding the next generation of nanomedicine designs.

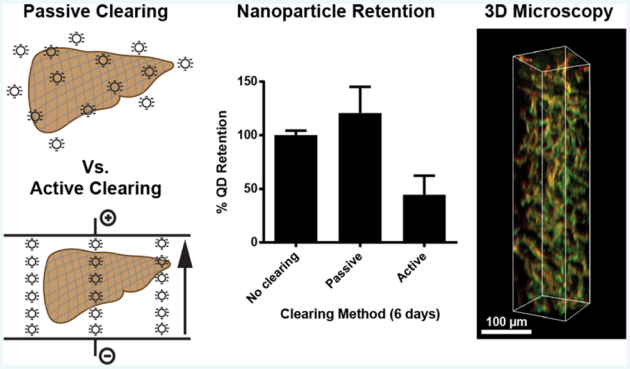

INTRODUCTION

Nanoparticles have the potential to deliver therapeutic agents to specific cells in the body, but they face several biological barriers before they can reach their target.[1] These barriers include the transport of nanoparticles through blood vessels, epithelial membranes, extracellular matrix, and certain cell types.[2,3] New techniques are required to study the interface between nanoparticles and biological barriers in three dimensions (3D). This would enable researchers to better understand how to overcome these biological barriers to enhance nanoparticle delivery. Currently, the use of techniques for optical imaging of intact tissue samples is limited. The reason for this is that visible and ultraviolet light is strongly scattered at the aqueous−lipid interface due to changes in refractive indices between these two media. This physical limitation only allows optical visualization of a few cell layers (~100 μm in the z-direction).[4,5] Thus, optical imaging in 3D requires sample transparency to allow deep penetration of light. This is achieved using chemical and physical treatments to remove interfaces within the sample with varying refractive indices.[5−13] Previously, we adapted the CLARITY technique[13] to show that tissues containing nanoparticles could be rendered transparent using high-throughput electrophoresis-assisted removal of lipids (termed active clearing).[4] There was minimal loss of proteins from these tissues, which were cross-linked into a hydrogel matrix. Nanoparticles were also retained during this process through the cross-linking of proteins adsorbed to their surface. This allowed high-resolution 3D mapping of nanoparticle distribution in intact liver, kidney, and spleen tissues. However, we still observed a substantial loss of nanoparticles: ~30% overall after 4 days of active clearing.[4] This loss is expected to increase with longer active clearing times. Although this extent of clearing was sufficient for imaging liver and

Special Issue: Interfacing Inorganic Nanoparticles with Biology

Received: September 6, 2016
Revised: October 27, 2016
Published: November 1, 2016

DOI: 10.1021/acs.bioconjchem.6b00500
Bioconjugate Chem. 2017, 28, 253−259

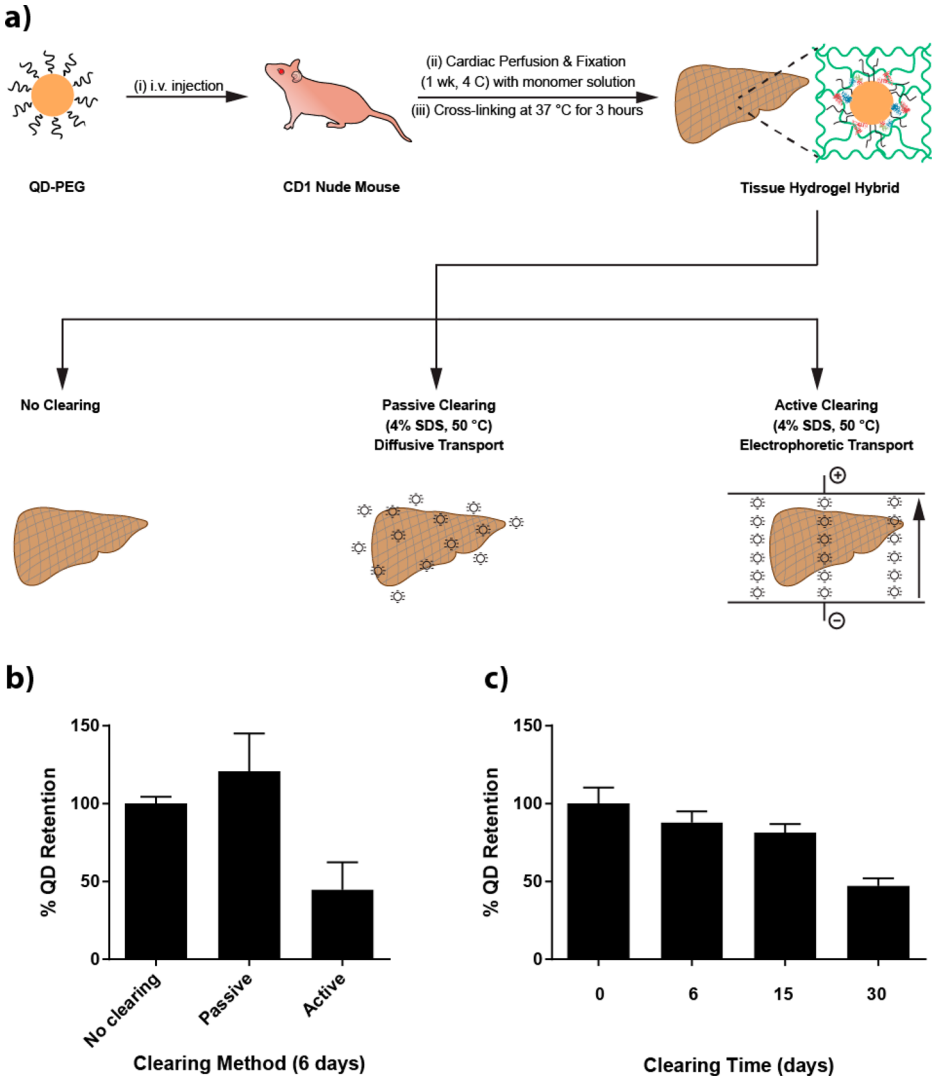

Figure 1. QD-PEG retention increase with passive clearing and decrease with increasing clearing time. (a) QD-PEG (590 nm emitting) were injected into mice intravenously via tail vein. PBS and cold hydrogel monomer solutions were perfused through the heart. This was followed by incubation in monomer solution and gelling to form cross-linked tissue hydrogel hybrids. Livers were excised, and lobes were either not cleared or cleared using active and passive clearing for quantifying retention of QD-PEG. (b) In comparison to tissues that were not cleared, passive clearing performed better by retaining nearly all of the QD-PEG, in contrast to 45% retention obtained using active clearing. (c) QD-PEG loss increased with increasing clearing time under passive clearing and reached the level of QD-PEG loss with 6 days of active clearing at 30 days. Mean ± standard deviation (n = 3) was used.

kidney, which require shorter clearing times, other tissues such as skin and xenograft tumors require longer clearing times to become optically transparent. This may lead to further loss of nanoparticles, which will cause complications in analysis due to imaging signal being below detection. Here, we explored the effect of clearing time and electrophoresis on the retention of nanoparticles, depth of imaging, and final image quality. We surprisingly found the use of passive clearing (rather than electrophoresis) led to a substantial increase in nanoparticle retention (88% of nanoparticles retained) with minimal difference in clearing time and improved image quality for nanoparticle detection.

RESULTS AND DISCUSSION

We first tested whether nanoparticle retention was sensitive to electrophoresis during the clearing process. For this purpose, we chose quantum dots that were surface functionalized with methoxy polyethylene glycol (QD-PEG) as model nanoparticles because their concentration can be quantified using elemental analysis and because they possess intrinsic fluorescence for visualizing their tissue distribution. In addition, their small size (6.4 ± 1.0 nm diameter) and high PEG surface density lead to lower protein adsorption than most other nanoparticle types (2×10^{-19} g of protein per particle, equivalent to the mass of approximately one albumin molecule).[4] As a result, QD-PEG is expected to have a lower level of cross-linking and retention in tissues compared to most other hard nanoparticles and therefore serves as a strict test for tissue treatment protocols for this application. We injected 400 pmoles of QD-PEG intravenously into CD1 Nude mice and allowed the nanoparticles to circulate for 72 h post-injection (Figure 1a). We then perfused 60 mL of saline solution (1× phosphate buffered saline, 0.5% sodium nitrite, and 10 U/mL of heparin) followed by 60 mL of cold fixative solution (2% acrylamide, 4% formaldehyde, 1× phosphate buffered saline, and 0.25% 2,2′-azobis[2-(2-imidazolin-2-yl)propane]-

DOI: 10.1021/acs.bioconjchem.6b00500
Bioconjugate Chem. 2017, 28, 253−259

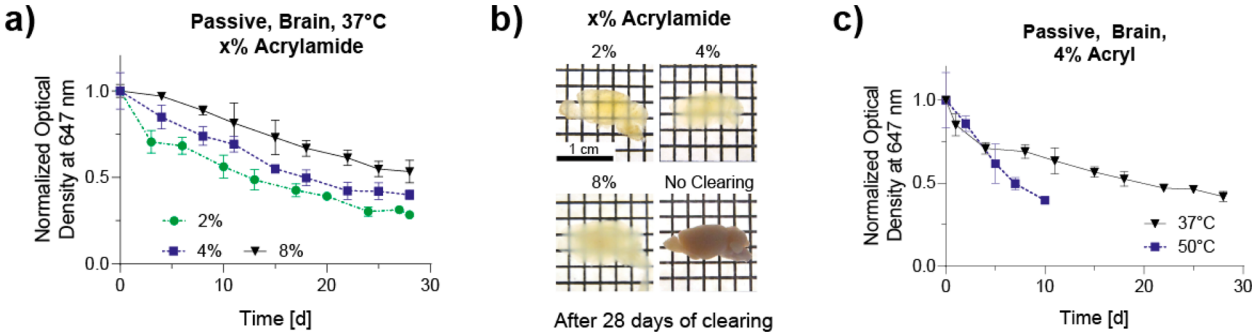

Figure 2. Effect of lowering acrylamide concentration and increasing temperature on the comparable rate of clearing. (a) The rate of clearing for brain hemispheres decreased with increasing acrylamide concentration (2−8%) in hydrogel monomer solution in passive clearing. (b) Upon raising of the temperature to 50 °C, the time to the end point absorbance was decreased ∼3 fold (10 days vs 28 days). Tissue optical density (OD) was normalized to the absorbance of the section after gelling and before any clearing was initiated. Measurement and analysis was performed using methods established previously.[4] (c) Representative photographs show the increased transparency with decreasing acrylamide concentration upon clearing for 28 days and subsequent index matching using RIMS. Mean ± standard deviation (n = 3) was used.

dihydrochloride initiator) (Figure 1a). We excised organs and further incubated them with the same hydrogel monomer solution for another week to form amide bonds between proteins, formaldehyde, and acrylamide. This was followed by the activation of the thermal initiator at 37 °C to polymerize acrylamide and cross-link tissues. We then cut the livers into similarly sized segments and subjected these segments to either active clearing or simple incubation with clearing solution (4% sodium dodecyl sulfate and 200 mM sodium borate (pH 8.5); termed passive clearing) for 6, 15, and 30 days (Figure 1a). We then measured the QD-PEG retained within cleared tissues using elemental analysis of cadmium(II) ions through inductively coupled plasma mass spectrometry (ICP-MS) and compared it to control tissues, which were not subjected to clearing.[4,14] We found that QD-PEG retention was 45% ± 31% at 6 days for active clearing compared to 121% ± 42% for passive clearing (Figure 1b). In a separate experiment over the course of 30 days of passive clearing, QD-PEG retention decreased from 88% ± 12% at 6 days to 47% ± 8% at 30 days, which is similar to the retention for only 6 days of active clearing (45% ± 31%). Taken together, this suggests that both longer clearing times and electrophoresis increase the loss of nanoparticles from tissues. Although increased nanoparticle retention from passive clearing was encouraging, the loss of nanoparticles has to be balanced against the time required to render tissues transparent and the final transparency of the tissues and the quality of the final image. Therefore, we next set out to investigate how these parameters are affected by passive clearing.

We first looked at the time required to render tissues transparent using passive clearing. We modulated three parameters: (i) concentration of acrylamide in hydrogel solution (2−8%, increasing concentration allows greater protein cross-linking and has been used to expand tissues), (ii) temperature (37 versus 50 °C; higher temperature accelerates clearing but may denature proteins), and (iii) organ type with varying protein content (brain, liver, and kidney). We found that the rate of passive clearing increased 1.5-fold when the acrylamide concentration was decreased from 4% to 2% w/v (Figure 2a). We also found that brains cleared faster than kidney and liver tissues, which can be attributed to their lower protein content (Figure S1). Additionally, the rate of passive clearing increased 3-fold when the temperature was increased from 37 to 50 °C, which can also be attributed to faster diffusion of SDS micelles. This means that brain tissues could be rendered transparent in ∼7 days by clearing at 50 °C and using 2% acrylamide for hydrogel embedding. Surprisingly, these results were not significantly slower than those previously obtained using active clearing,[4] suggesting that electrophoresis does not have a large impact on the time required for clearing when used at 25 V with the design we employed. Other research groups have observed faster clearing in head-to-head comparisons, but these strategies have used either larger electrode surface areas, higher voltages, higher temperatures, or more-complicated strategies for enhancing the local electric field, which dramatically increases the costs and labor associated with electrophoretic clearing.[10,13] Active clearing used here requires 13.2 g of platinum wire and 4 kg of SDS (for clearing 48 tissues) in addition to other electrical and material supplies to clear 48 tissues simultaneously. Furthermore, we replaced 13 L of clearing solution every day as the pH changed from 8.5 to 7 because further acidification may be detrimental to protein structure and stability. In comparison, passive clearing does not require any platinum and utilizes 10-fold less SDS without daily replacement. These complications and larger electrode surfaces limit the scalability and practicality of active clearing when applied to large numbers of samples simultaneously.

Another possible concern with changing the mode of clearing from active to passive is the resulting quality and depth of imaging. We investigated this by staining cleared tissues for cellular nuclei using small molecular stains. Nuclear stains are desirable for evaluating imaging depth because they generate reproducible and dense labeling of all tissues, which allows quantitative comparisons. Specifically, we first obtained cylindrical blocks of cleared tissues using a biopsy punch (diameter of 4 mm) because smaller tissue samples require shorter staining times (Figure 3a). We then stained these blocks with fluorescent nuclear stains, either SYTOX Green (ex/em: 504/523 nm) or TOTO-3 (ex/em: 640/660 nm), at a concentration of 100 pmol of dye for each milligram of tissue for 4 days at 37 °C (Figure 3a). We then imaged the fluorescence from these blocks using confocal fluorescence microscopy using a 10× objective (NA = 0.45). In confocal microscopy, optical scattering blurs the fluorescent signal from the tissue and this effect increases along the z-axis because both excitation and emission signals need to go through more layers of tissue. Typically, individual nuclei could easily be distinguished at the surface of the tissue closer to the objective

DOI: 10.1021/acs.bioconjchem.6b00500
Bioconjugate Chem. 2017, 28, 253−259

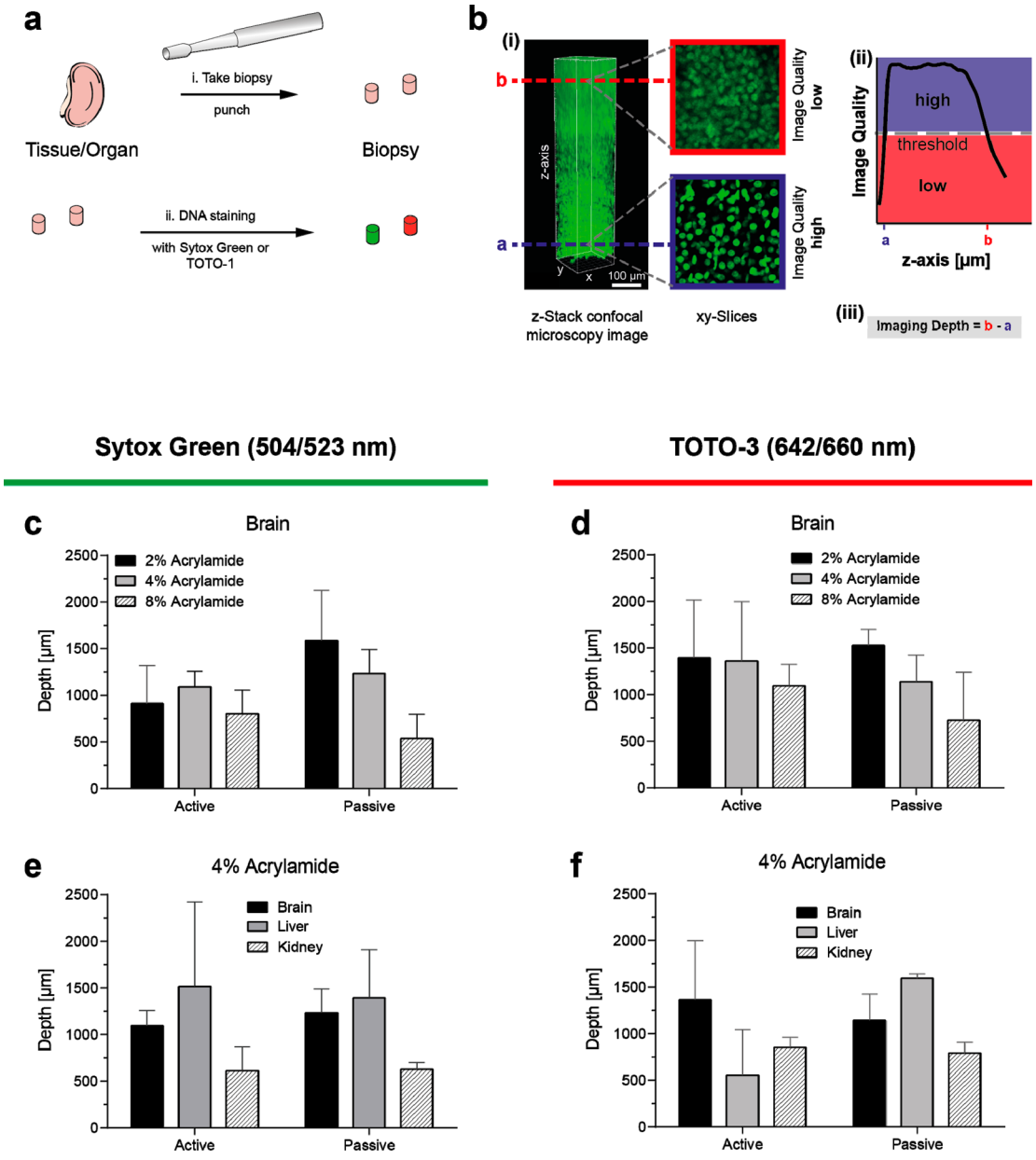

Figure 3. Quantification of imaging depth tissues after passive clearing. (a) Tissues were sectioned into a cylindrical block and stained using either SYTOX Green (ex/em: 504/523 nm) or Toto-1 (ex/em: 640/660 nm). (b) (i) Each tissue block was imaged using confocal microscopy. Single cells can be visualized with high imaging quality near the surface of the tissue (labeled a in the image). However, as imaging depth increases, the signal-to-noise decreases, leading to low imaging quality (labeled b in the image). (ii) BRISQUE-based assessment of imaging quality allows the determination of imaging depth by the selection of a cutoff score (labeled as threshold) of 50. (iii) The imaging depth can thus be calculated by subtracting the *z*-axis positions (b − a) for these levels. (c,d) Brain hemispheres with varying acrylamide concentration and (e,f) different organs (brain, livers, and kidneys) were stained, imaged, and analyzed to obtain imaging depth. Mean ± standard deviation (n = 3) was used.

(labeled a in Figure 3b; objective located below the stack shown) but are difficult to differentiate at higher positions (labeled b). We analyzed the quality of these 3D images along the *z*-axis with a blind image quality assessment algorithm, BRISQUE (see the Experimental Procedure section for details), to quantify the effect of scattering in each block (Figure 3b). By setting a quality threshold of 50 points from the BRISQUE algorithm (Figure 3bii), we obtained the depth of imaging for each block (Figure 3biii). Among tissues cleared for 28 days, we found that imaging depth decreases for passive clearing with increasing acrylamide concentration but found no difference with active clearing (Figure 3c,d). Similarly, imaging depth decreases from brains and livers to kidneys for passive clearing (Figure 3e,f), which corresponds to the extent of clearing for tissues with higher protein content. Importantly, there was no significant difference between active and passive clearing in terms of the final imaging quality and depth. Combined with previous results, this suggests that passive clearing is more suitable for imaging nanoparticles in tissues because of higher nanoparticle retention, simpler processing and no significant differences in the time required for clearing or the final imaging quality. We next tested whether these advantages of passive clearing translated into visualization of nanoparticles in 3D across different organs.

To validate that visualization of nanoparticles in 3D can be achieved with optimized passive clearing conditions, mice were

DOI: 10.1021/acs.bioconjchem.6b00500
Bioconjugate Chem. 2017, 28, 253−259

first injected with 4 nmoles of QD-PEGs and allowed to circulate for 72 h. Tissues were perfused and cleared passively for 6 days at 50 °C with 2% acrylamide hydrogel solution. In a liver tissue cleared passively, both QD-PEG and blood vessels could be visualized, which has previously been demonstrated with active clearing (Figure 4a) with a BRISQUE score of

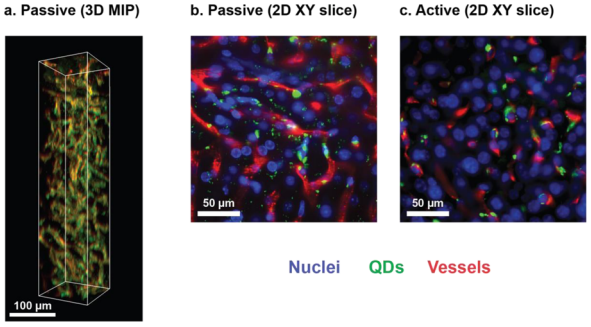

Figure 4. Higher retention with optimized passive clearing compared to active clearing and higher sensitivity for visualizing nanoparticles in 3D. (a) 3D maximum intensity projection of liver cleared optimized passive clearing conditions with labeled blood vessels (red) and QD-PEG (green). (b,c) 2D XY projection of images of (b) passively and (c) actively cleared liver with nuclei labeled with DAPI (blue) in addition to blood vessels (red) and QD-PEG (green). Higher retention in passively cleared liver reveals some QD-PEG signal within hepatocytes and bile canaliculi, which are indicative of hepatobiliary clearance. These signals are not present within the actively cleared liver.

greater than 50 throughout the stack, ensuring high image quality (Figure S2). However, examining the 2D slices comprising these images showed a number of spots positive for QD-PEG signal located within hepatocytes, which may indicate hepatobiliary clearance but this was observed only in the liver cleared using passive clearing (Figure 4b). In the slice cleared using active clearing, this could not be observed presumably because the weaker signal from QD-PEG in this tissue prevented the detection of these faint spots (Figure 4c). This suggests that improved retention of nanoparticles in tissues due to the elimination of the electrophoresis step may lead to new biological insights about nanoparticle distribution in tissues.

CONCLUSIONS

In summary, we have developed a 3D nanoparticle mapping methodology that retains nearly all the nanoparticles in the tissue. This is important because nanoparticle clearance through hepatobiliary or renal systems and nanoparticle accumulation in disease models such as tumors may involve only a small fraction of the total dose of injected nanoparticles. This small dose may not be detectable if the clearing techniques employed lose a significant proportion of nanoparticles or if the imaging technique lacks the necessary sensitivity. We found that 3D imaging of nanoparticles in tissues was improved using passive clearing of tissues compared to active clearing due to improved retention of nanoparticles. Systematic investigation of clearing parameters showed that this method did not result in a longer clearing time or in reduced imaging depth. We were surprised with our findings for passive clearing as we started by developing the active clearing process for characterizing nanoparticle−tissue interaction. Our characterization of the passive process simplifies the entire clearing scheme for nanomedicine researchers. We will further explore where active clearing may be useful (e.g, tissue staining or larger tissues). The optimization and evaluation of clearing techniques for applications in nanomedicine is critical to understanding the role of 3-D architecture in mediating nanoparticle−biological interactions or elucidating the impact of therapies on tissue structures. Our protocols for passive clearing will enable researchers to easily implement tissue clearing in a common laboratory settings with the most accurate nanoparticle localization and image quality for understanding the interface between materials and intact biological environments.

EXPERIMENTAL PROCEDURE

Quantum Dot Surface Modification with PEG and Characterization. Alkyl surface functionalized Trilite CdSeS quantum dots (590 nm emission, CrystalPlex, Pittsburgh, PA) were modified with 5 kDa sulfhydryl-mPEG (Laysan Bio MPEG-SH-5000), as described previously.[4,14] A two-step ligand exchange method was used to PEGylate quantum dots. A total of 130 μL of stock QD solution (25 mg/mL) was mixed with 425 μL of chloroform and 900 μL of thioglycolic acid (Sigma T3758) and stirred for 7 h at room temperature for the first ligand exchange. Quantum dots (QDs) were precipitated from this mixture by adding equal volume of acetone containing 1.85 wt % tetramethylammonium hydroxide pentahydrate (Sigma T7505) and isolated by centrifugation at 1000 *g* for 5 min. This acetone washing was repeated three times. The second ligand exchange was performed by adding excess mPEG-SH 5 kDa (QD-to-mPEG molar ratio of 1:11250) in 50 mM borate buffer (pH 8.5) at 60 °C for 60 min. These QD-PEG were purified from unreacted PEG by using 50 kDa Amicon Ultra centrifugal filters.

Fluorescent Labeling of *Griffonia simplicifolia* Lectin 1 (GSL-1, for Blood Vessel Staining) with Alexa Fluor 647 NHS. The conjugation and purification procedure for fluorescent labeling of *G. simplicifolia* Lectin 1 (Vector Laboratories) with Alexa Fluor 647 (Invitrogen) was adapted from work described previously.[4] A total of 100 μL of 10 mg/mL unconjugated GSL-1 (100 mM sodium bicarbonate buffer; pH 8.3) was added to 100 μg of lyophilized Alexa Fluor 647 NHS ester. The mixture was incubated overnight with gentle vortexing at room temperature. The conjugate was purified by size exclusion chromatography using a NAP-5 column (Sigma GE17-0853-01). It was then washed and concentrated using Amicon 30 kDa cutoff centrifugal filters (Millipore, UFC500324). The degree of labeling was determined by measuring absorbance at 647 and 260 nm after completing purification and concentration steps, as published previously.[4] Degree of labeling varied between 4−6 AF647 molecules per GSL-1.

Quantum Dot and GSL1-A647 Administration in Animals. QD-PEG solutions (in 1× sterile PBS) were injected intravenously via tail vein into 8 week old CD1 nude mice with a 150 uL volume at 400 pmol/animal (7.6 mg/kg) for nanoparticle retention quantification and at 4000 pmol/animal (76 mg/kg) for whole-organ imaging. The QD-PEG were allowed to circulate for 72 h for organ distribution and cellular uptake. Blood vessels were stained with a 150 μL tail-vein injection of GSL1-Alexa647 (1 mg/mL) 5 min prior to cardiac perfusion.

Transcardial Perfusion Fixation. Before initiating the surgical procedure for cardiac perfusion, mice were anaesthetized using a continuous flow of 3% isoflurane mixed with

DOI: 10.1021/acs.bioconjchem.6b00500
Bioconjugate Chem. 2017, 28, 253−259

oxygen. Transcardial perfusion[4,15] was performed to remove blood and distribute hydrogel components in tissues. This technique is carried out by inserting the needle carrying perfusate into the left ventricle of the mouse heart and making an incision in the right atrium to drain the fluid. First, blood was removed by transcardial perfusion (5.5 mL/min) of 60 mL of solution containing PBS (1×, Bioshop Canada Inc.), heparin (10 U/mL, Bioshop), and sodium nitrite (0.5% w/v, Sigma-Aldrich). This was followed by 60 mL of the hydrogel monomer solution. This solution consists of 4% formaldehyde (Sigma-Aldrich), 1× PBS, 0.25% initiator (VA-044 azoinitiator, Wako Chemicals), and either 2%, 4%, or 8% acrylamide (Bioshop Canada Inc.). Brains were resected and bisected to minimize animals and obtain large number of samples. Liver lobes and a whole kidney were isolated for clearing.

Polymerization of Hydrogel. Harvested tissues were incubated in 50 mL Falcon tubes for another week, with hydrogel monomer solutions matching the perfused solution. This incubation was done at 4 °C for 7 days with gentle shaking to ensure uniform distribution of chemicals. The solution was replaced with fresh hydrogel monomer solution before carrying out polymerization for gelling. The caps of the falcon tubes were replaced with a cap with two small holes (using a 1/16 in. drill). The holes were made to degas tissues by placing the falcon tubes inside a desiccator. The tubes underwent three vacuum cycles followed by purging with argon. Upon opening the desiccator lid, the caps were covered with parafilm quickly to minimize the replacement of argon with oxygen. The tubes were incubated at 37 °C for 3 h to activate the initiator and polymerize acrylamide gel within the tissue. Excess gel was removed and discarded. The samples were stored in borate buffer (200 mM sodium borate, pH 8.5, 0.1% Triton-X100, and 0.01% sodium azide) at 4 °C until further processing.

Passive and Active Clearing. Tissues were cleared as whole organs, half organs or sectioned using a 1 mm steel matrix (Zivic Instruments). These tissues were cleared passively with solution consisting of 4% w/v SDS and 200 mM sodium borate at pH 8.5. Clearing was carried out either at 37 or 50 °C. For thin 1 mm slices, 15 mL of clearing solution was used, whereas for whole or half organs, 50 mL of solution was used. The solution was replaced twice a week. For active clearing, samples were cleared using electrophoresis as published previously.[4]

End-Point Processing. For parametric evaluation of clearing, the tissues were cleared for 28 days or after achieving normalized optical density (OD) of <0.33. During this time, tissues were incubated at 37 °C with daily replacement of clearing solution. Once clearing was finished, tissues were incubated with 3−5 mL of RIMS solution (88% iohexol, 2.5% 1,4-diazabicyclo[2.2.2]octane, 50 mM sodium borate (pH 8.5), and 0.01% sodium azide) and incubated at 37 °C.

Optical Density Measurement during Clearing. The extent of clearing was tracked by measuring the optical density of tissues every 2 days in RIMS solution. This optical density of tissues was measured using the custom tracing algorithm as mentioned previously.[4]

Tissue Sampling and Staining. After tissues were cleared and leftover SDS had been washed using borate buffer, nuclear staining was done with DAPI or SYTOX Green (Life Technologies, ex/em: 504/523 nm). These dyes were prepared at a concentration of 10 μM solution, and tissue staining was carried out for 4 days at 37 °C with 100 pmol of dye per mg of cleared tissue in borate buffer. Excess dye was washed by rinsing in 1 mL of borate buffer for 1 day at 37 °C. The refractive index of tissues was matched with either RIMS or 67% aqueous solution of 2′2-thiodiethanol (TDE) solution.

3D Tissue Imaging. Imaging of tissues containing nanoparticles and for evaluating depth of imaging was done using a Zeiss Lightsheet Z.1 microscope (Clr Plan-Neofluor Objective: 20×, NA = 1, refractive index of 1.45) and Nikon Confocal Microscope (Apo Plan Air Objective: 10×, NA = 0.45). After images were acquired, Bitplane Imaris was used to prepare movies and 3D images.

Image Analysis. Confocal 3D images were imported into MATLAB, and the quality score was determined using BRISQUE[16] for each XY slice along the *z*-direction. *Z*-direction is taken as the direction moving into tissue. Imaging depth was calculated based on the number of consecutive *xy* slices with a quality score greater than 50.

ICP-MS for Quantitative Biodistribution and Quantum Dot Retention. Retention of nanoparticles in tissues was quantified using elemental analysis of cadmium (from QD-PEG). Sections of liver with approximately the same mass were cleared under various passive and active conditions. Uncleared tissues served as the control. The tissues were digested in 15 mL Falcon tubes with 0.8 mL of nitric acid and 0.2 mL of hydrochloric acid for 30 min at 70−90 °C to completely solubilize tissues. The tubes were covered loosely to trap heat and accelerate digestion. The samples were then diluted to 40 mL with deionized water. A total of 10 mL of this solution was filtered through a Millipore 0.22 μm PVDF filter to remove any debris. Cadmium standards were prepared in the range of 100−0.001 mg/mL, as published.[4] Elemental analysis was performed using a PerkinElmer NexION ICP-MS system, which has an inline iridium as the internal standard.

■ ASSOCIATED CONTENT

Supporting Information

The Supporting Information is available free of charge on the ACS Publications website at DOI: 10.1021/acs.bioconjchem.6b00500.

Figures showing the clearance of various tissues and transparency after refractive index matching and image quality scores as a function of imaging depth. (PDF)

■ AUTHOR INFORMATION

Corresponding Author

*E-mail: warren.chan@utoronto.ca.

Author Contributions

#S.S. and A.M.S. contributed equally to this work.

Notes

The authors declare no competing financial interest.

■ ACKNOWLEDGMENTS

We acknowledge the Canadian Institutes of Health Research (CIHR) and Natural Sciences and Engineering Research Council (NSERC) for supporting the project. S.S. acknowledges CIHR, and A.M.S. acknowledges NSERC for student fellowship.

■ REFERENCES

(1) Kim, B. Y. S., Rutka, J. T., and Chan, W. C. W. (2010) Nanomedicine. *N. Engl. J. Med. 363*, 2434−2443.

(2) Park, K. (2013) Facing the Truth about Nanotechnology in Drug Delivery. *ACS Nano 7*, 7442−7447.

DOI: 10.1021/acs.bioconjchem.6b00500
Bioconjugate Chem. 2017, 28, 253−259

(3) Wilhelm, S., Tavares, A. J., Dai, Q., Ohta, S., Audet, J., Dvorak, H. F., and Chan, W. C. W. (2016) Analysis of nanoparticle delivery to tumours. *Nat. Rev. Materials 1*, 16014.
(4) Sindhwani, S., Syed, A. M., Wilhelm, S., Glancy, D. R., Chen, Y. Y., Dobosz, M., and Chan, W. C. W. (2016) Three-Dimensional Optical Mapping of Nanoparticle Distribution in Intact Tissues. *ACS Nano 10*, 5468−5478.
(5) Kim, S.-Y., Chung, K., and Deisseroth, K. (2013) Light microscopy mapping of connections in the intact brain. *Trends Cognit. Sci. 17*, 596−599.
(6) Tainaka, K., Kubota, S. I., Suyama, T. Q., Susaki, E. A., Perrin, D., Ukai-Tadenuma, M., Ukai, H., and Ueda, H. R. (2014) Whole-Body Imaging with Single-Cell Resolution by Tissue Decolorization. *Cell 159*, 911−924.
(7) Chung, K., and Deisseroth, K. (2013) CLARITY for mapping the nervous system. *Nat. Methods 10*, 508−513.
(8) Murray, E., Cho, J. H., Goodwin, D., Ku, T., Swaney, J., Kim, S.-Y., Choi, H., Park, Y.-G., Park, J.-Y., Hubbert, A., et al. (2015) Simple, Scalable Proteomic Imaging for High-Dimensional Profiling of Intact Systems. *Cell 163*, 1500−1514.
(9) Yang, B., Treweek, J. B., Kulkarni, R. P., Deverman, B. E., Chen, C.-K., Lubeck, E., Shah, S., Cai, L., and Gradinaru, V. (2014) Single-Cell Phenotyping within Transparent Intact Tissue through Whole-Body Clearing. *Cell 158*, 945−958.
(10) Tomer, R., Ye, L., Hsueh, B., and Deisseroth, K. (2014) Advanced CLARITY for rapid and high-resolution imaging of intact tissues. *Nat. Protoc. 9*, 1682−1697.
(11) Ertürk, A., Becker, K., Jährling, N., Mauch, C. P., Hojer, C. D., Egen, J. G., Hellal, F., Bradke, F., Sheng, M., and Dodt, H. U. (2012) Three-dimensional imaging of solvent-cleared organs using 3DISCO. *Nat. Protoc. 7*, 1983−1995.
(12) Chen, F., Tillberg, P. W., and Boyden, E. S. (2015) Expansion microscopy. *Science 347*, 543−548.
(13) Chung, K., Wallace, J., Kim, S.-Y., Kalyanasundaram, S., Andalman, A. S., Davidson, T. J., Mirzabekov, J. J., Zalocusky, K. A., Mattis, J., Denisin, A. K., Pak, S., et al. (2013) Structural and molecular interrogation of intact biological systems. *Nature 497*, 332−337.
(14) Sykes, E. A., Dai, Q., Tsoi, K. M., Hwang, D. M., and Chan, W. C. W. (2014) Nanoparticle exposure in animals can be visualized in the skin and analysed via skin biopsy. *Nat. Commun. 5*, 3796.
(15) Gage, G. J., Kipke, D. R., and Shain, W. (2012) Whole Animal Perfusion Fixation for Rodents. *J. Visualized Exp. 65*, e3564.
(16) Mittal, A., Moorthy, A. K., and Bovik, A. C. (2012) No-Reference Image Quality Assessment in the Spatial Domain. *IEEE Trans. on Image Process 21*, 4695−4708.

DOI: 10.1021/acs.bioconjchem.6b00500
Bioconjugate Chem. 2017, 28, 253−259